

Continuous Health Monitoring of Rolling Element Bearing Based on Nonlinear Oscillatory Sample Entropy

Khandaker Noman¹, Yongbo Li², *Member, IEEE*, and Shun Wang³

Abstract—As a nonlinear measure, sample entropy (SE) can be considered a suitable parameter for characterizing rolling element bearing health status by measuring complexity of vibration signals. However, in continuous monitoring scenario under noisy condition, all components of a multicomponent bearing signal are not equally sensitive toward change of SE value. As a consequence, a direct application of SE results in inefficient early fault warning and inability to differentiate among different fault types. To deal with this problem, instead of direct utilization of a whole vibration signal, its principal component (PC) sensitive to SE calculation is separated with the help of continuously adjustable parameterized tunable Q factor wavelet transform (TQWT). Since TQWT uses an oscillation-based bearing PC separation scheme for SE calculation, the newly proposed measure is termed as oscillatory sample entropy (OSE). Due to the biasness of SE algorithm toward bearing PC, the proposed OSE can anticipate theoretical concept of complexity change more efficiently with the change of bearing health. Two experimental case studies have shown that proposed OSE can not only overcome the limitations of SE algorithm but also demonstrate superiority over approximate entropy (AE) and fuzzy entropy (FE) for continuous monitoring of bearing health.

Index Terms—Continuous health monitoring, nonlinear measure, sample entropy (SE), tunable Q -factor wavelet transform (TQWT).

I. INTRODUCTION

ROLLING element bearings are susceptible to various kinds of faults during industrial application due to their exposure to the harsh working environment such as simultaneous influence of heat, corrosion, extreme load, and so on [1]. Being an integral part of the modern machineries, bearing failures may result in large financial losses or even catastrophic scenario [2]. Hence, prognosis of rolling element bearing health has drawn particular attention from the researchers in the past few years. In this context, vibration-based condition monitoring of rolling element bearing is the most effective strategy due to high sensitivity of vibration signals toward

bearing health and convenience of data collection with the help of accelerometer [3].

This monitoring of rolling element bearing health with an efficient measure is a major aspect of the prognosis operation. In this regard, early detection of bearing fault is the most important trait of the measure employed for its health monitoring [4]. Hence, it can be realized that construction of a successful bearing health monitoring index is the main theme of bearing health prognosis. As fault information of bearing is mostly reflected by singular points of abrupt changing signals, detecting dynamic change of vibration signals in time is important for early fault identification [5]. Moreover, in real life applications, vibration signals collected from rolling element bearings are highly nonstationary and nonlinear in nature due to the association of external force, friction, environmental noise, and so on [6]. As a result, construction of nonlinear health monitoring indices for rolling element bearing has drawn particular attention among the researchers. In this context, different nonlinear dynamic measures such as Lyapunov exponent [7], correlation dimension [8], symbolic dynamics [9] have been used by different researchers. However, these methods are dependent on the quantification of certain aspects in the phase space which is inefficient in terms of calculation. In this context, entropy-based measures play a significant role in characterizing a time series continuously in a dynamic process [10], [11]. The concept of information entropy was laid by Shannon in 1948 [12]. Following his concept, aiming at solving the short length problem of the entropy calculation of a finite time series, Pincus proposed approximate entropy (ApEn) [13]. However, one of the major disadvantages of ApEn is its self-matching limitation. Later, Bandt and Pompe [14] proposed permutation entropy (PE) to address the self-matching limitation of ApEn. However, PE cannot classify well defined pattern of a particular design [6].

Free from the weaknesses of already mentioned entropy methods, sample entropy (SE) is a suitable alternative for continuous monitoring of bearing health [13]. However, a direct application of SE suffers from contamination by surrounding noise. A high value of SE can either represent the contamination by heavy noise or inception of a fault. This problem is more prominent at the initial stage of fault inception when the amplitudes of fault impulses are relatively small. A high value of SE can either interpret the deterioration of bearing health or heavy noise. In this regard, an improved version of SE is

Manuscript received 17 January 2022; revised 4 May 2022; accepted 29 June 2022. Date of publication 20 July 2022; date of current version 28 July 2022. This work was supported in part by the National Natural Science Foundation of China under Grant 12172290 and in part by the Key Laboratory of Equipment Research Foundation under Grant 6142003190208. The Associate Editor coordinating the review process was Dr. Loredana Cristaldi. (*Corresponding author: Yongbo Li.*)

The authors are with the School of Aeronautics, Northwestern Polytechnical University, Xi'an 710072, China (e-mail: khandakernoman93@nwpu.edu.cn; yongbo@nwpu.edu.cn; wangshun@mail.nwpu.edu.cn).

Digital Object Identifier 10.1109/TIM.2022.3191712

1557-9662 © 2022 IEEE. Personal use is permitted, but republication/redistribution requires IEEE permission.
See <https://www.ieee.org/publications/rights/index.html> for more information.

proposed based on the multiscale analysis [15]. Nevertheless, Multiscale sample entropy (MSE) is mostly dependent on the use of a suitable classifier for performing health monitoring of a bearing. In this context, classifier efficiency depends on past data for training relevant algorithms [16], [17]. Hence, this approach requires additional storage facility for these past data and subjected to proper data management for bearing operating under different working conditions. Moreover, in conventional SE-based bearing health monitoring process, additional operation such as manual inspection or envelope spectrum analysis is needed for identifying the type of incepted fault. However, this type of approach is dependent on the prior knowledge about bearing specification in order to know relevant bearing fault frequency. Hence, this is not suitable in a continuous monitoring process specially in the real-life industrial application where bearings with different specifications are utilized. Considering the aforementioned limitations of SE in continuous monitoring of rolling element bearing health, two main contributions of this manuscript are as follows.

- 1) A new variant of SE algorithm is designed which can detect the fault at an early point of inception.
- 2) Automatic identification of unknown bearing fault type has been achieved during continuous health monitoring process.

Before analyzing a bearing signal by any entropy algorithm, it is required to extract the most effective part of that signal. As a result, researchers have applied SE for condition monitoring of rolling element bearing after preprocessing the bearing signal with the help of different preprocessing techniques [18]–[20]. However, conventional wavelet-based preprocessing techniques are dependent on a fixed scale of a base function in order to perform the denoising operation which is not very suitable for applying in the continuous monitoring operation [21]. Alternatively, adaptive decomposition-based methods, such as empirical mode decomposition (EMD), local mean decomposition (LMD), and so on, suffer from mode mixing problem [22]–[24]. Even though utilization of additional white noise can address the mode mixing problem, they are not suitable solution due to their dependence on the predefined parameters [23], [25], [26]. In the context of the above discussions, tunable Q factor wavelet transform (TQWT) is a relatively new signal preprocessing technique proposed by Selesnick [27]. Being a continuously tunable parameterized method, a signal can be decomposed into high and low oscillatory component with the help of TQWT. As a result, it is suitable for a process requiring continuous monitoring. Recently, TQWT has drawn considerable attention among researchers regarding bearing fault diagnosis [28]–[34].

On the basis of all above, in this article, Section II describes limitations of original SE algorithm in continuous monitoring of bearing health with the help of numerical simulated signals. In Section III, firstly, biasness of SE toward bearing principal component (PC) is studied. Then, in order to utilize the advantages of this finding, in lieu of calculating the original SE algorithm directly for bearing health monitoring, TQWT is implemented to separate corresponding bearing PC for calculating its SE value. Due to the dependence on oscillation-based

PC separation scheme, the proposed measure is termed as oscillatory sample entropy (OSE). Experimental validation has been done in Section IV. Lastly, Section V discusses the conclusions of this article.

II. THEORY OF SE AND ITS LIMITATIONS IN CONTINUOUS MONITORING OF BEARING HEALTH

SE was proposed by Richman and Moorman [13] as a measure of complexity computation of a time series. Low SE value infers lower irregularity of a time domain signal and vice versa.

A. Theory of SE Algorithm

Mathematical theory of SE is provided in detail in [13]. For a time series $S = \{S(1), \dots, S(i), \dots, S(N)\}$ of length N , detailed steps of calculating SE are as follows.

Step 1: m embedding vectors are constructed according to the Taken's theorem as shown in the following equation:

$$S_i^m = \{S_i, S_{i+1}, \dots, S_{i+m-1}\}, \quad 1 \leq i \leq N - m. \quad (1)$$

Step 2: If two vectors S_i^m and S_j^m are equal where $i \neq j$, then (S_i^m, S_j^m) are termed as m -dimensional matched vector pair. The total number of matched vector pairs are considered as n^m for embedding dimension m .

Step 3: Steps 1 and 2 are repeated for embedding dimension $m = m + 1$ which is resulted in the n^{m+1} number of matched vector pairs.

Step 4: SE is calculated based on the following equation:

$$SE(S, m) = -\ln \frac{n^{m+1}}{n^m}. \quad (2)$$

B. Limitations of SE in Continuous Monitoring of Bearing Health

Limitations of the SE algorithm in relevance to monitoring of bearing health in a continuous manner are studied in this section with the help of numerical simulated signals.

Vibration signals corresponding to inner race fault, outer race fault, and rolling element fault are simulated by considering the effect of bearing geometry, shaft speed, load, and damping nature of impulses generated by fault [35]. Periodical impulses generated in the vibration signal due to the inception of fault can be modeled as

$$X_o(t) = \left[\sum_{k=-\infty}^{\infty} d_0 \delta(t - kT_0) \right] * e^{-Dt} \quad (3)$$

$$X_i(t) = \left\{ \left(\sum_{k=-\infty}^{+\infty} d_i \delta(t - kT_i) \right) * q(2\pi f_r t) * p(2\pi f_r t) \right\} * e^{-Dt} \quad (4)$$

where $X_o(t)$, $X_i(t)$, respectively, indicates the fault impulses generated by bearing outer race and inner race fault. d_0 and d_i , respectively, indicates the amplitude of impulses for outer and inner race fault. T_0 and T_i represents reciprocal fault characteristic values corresponding to bearing outer race and inner race, respectively. Radial load distribution of the rolling element is

represented by q and f_r represents the shaft rotating frequency. Exponential decaying nature of bearing fault impulses are obtained by e^{-Dt} where D is the damping coefficient. k represents the number of impulses and δ represents bearing fault impulse function.

In this article, shaft rotating speed f_r is considered as 50 Hz. Values of T_0 and T_i are considered as 0.0049 and 0.0034, respectively. Simulated signals are generated at a sampling frequency of 20 480 Hz. In this article, values of parameters related to original SE calculation are taken according to [36]. Two key limitations of original SE algorithm in continuous monitoring of bearing health are studied in this section below.

1) *Under Heavy Noise, Original SE Algorithm Is Insensitive to Bearing Fault Frequency:* In an ideal scenario, vibration signals collected from healthy bearing operating without influence of any additional excitement should have an SE value 0. However, in real application, vibration signals collected from rolling element bearing contain undesired frequency components such as frequency component related to unbalance, misalignment, rotation of rolling element, and so on. Because of the presence of these extra periodic components in bearing vibration signal, value of corresponding SE algorithm increases to more than 0. Also, during vibration data collection from a bearing shaft, it is almost impossible to avoid the association of random noise components. As a result, SE value of bearing vibration signal gets increased further. In this way, under extreme noisy conditions, SE value of a vibration signal collected from a normal healthy bearing approaches to its upper limit.

In this context, after the inception of fault in a bearing, change of SE value become insignificant due to the addition of corresponding fault frequency components. This is caused by negligible amount of fault frequency components in compare to that of environmental noise. Numerically simulated signals have been used in order to understand this phenomenon. A representative signal corresponding to a healthy bearing can be modeled by (5) as follows [10], [37]:

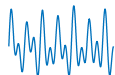


$$S(t) = 0.05 * \sin(2 * \pi * F_u * t) + 0.10 * \sin(2 * \pi * F_m * t) + 0.325 * \sin(2 * \pi * F_{BPFOR} * t) \quad (5)$$

where F_u , F_m , F_{BPFOR} , respectively, represent the frequency components corresponding to unbalance, misalignment, and passing of bearing rolling element periodically in relation to accelerometer fixing point on the casing. Values of F_u , F_m , and F_{BPFOR} are considered as 30, 60, and 41 Hz, respectively. The association of extra environmental noise $n(t)$ in the vibration data collection process has been taken into account while simulating the vibration signal corresponding to healthy condition as shown in the following equation:

$$S_{Healthy}(t) = S(t) + n(t). \quad (6)$$

During continuous operation of bearing, sudden emergence of faults adds some additional frequencies to the collected vibration data. In this context, firstly SE value of $S_{Healthy}(t)$ is calculated. Then, for understanding the change of SE due to occurrence of bearing fault, fault impulse generated by (3) or (4) can be added with the simulated healthy bearing signal.

TABLE I
CHANGE OF SE VALUES UNDER DIFFERENT HEALTH CONDITION

Signal	Signal time series	SE
$S(t)$		0.0708
$S_{Healthy}(t)$		≈ 1.7855
$\begin{cases} S_{Healthy}(t) + X_o(t) \\ S_{Healthy}(t) + X_i(t) \end{cases}$		≈ 1.7855

In order to simulate extremely noisy condition, Gaussian noise equivalent to -20 dB is considered. Corresponding SE values are presented in Table I.

From Table I, it can be observed that a healthy bearing signal without any noise has relatively small value of SE. However, with the addition of noise, its value becomes very high which remains very similar even after the addition of fault impulses in the signal. Hence, it can be said that under extreme noisy condition, original SE algorithm is insensitive toward the bearing fault frequency.

2) *SE Cannot Identify Among Different Fault Types During Continuous Monitoring Process:* The entropy value of a bearing signal time series is dependent on the amount of frequency components present in it [10], [37], [38]. During normal operation of a healthy bearing, contact pressure among different mating parts of a bearing remain unchanged. With the inception of fault in a bearing, corresponding contact pressure between relevant mating parts changes. This fluctuation in the contact pressure results in amplitude and frequency modulation which in turn also generates more frequency peaks and their harmonics [39].

When an outer race fault occurs in a bearing, real area of contact between mating parts becomes smaller due to the subtraction of size of the fault from nominal contact area. This results in the variation of the contact pressure between the fixed outer race fault and the rolling element. As a result, frequency modulation happens [39]. With the progression of fault, fluctuations of contact pressure become more intensified and related frequency modulation become more and more strong. This strengthening of the frequency modulation causes more and more frequency peaks and their harmonics in the frequency domain of the signal. Hence, it is expected that value of SE will increase with the progression of outer race fault.

On the contrary, for inner race fault, nonuniform load distribution, as shown in Fig. 1, caused by radial load plays a significant role in its entropy calculation.

As seen in Fig. 1, due to the influence of radial load, the point of contact expands to an ellipse. The maximum contact pressure P_{max} is located at the center of the ellipse and can be

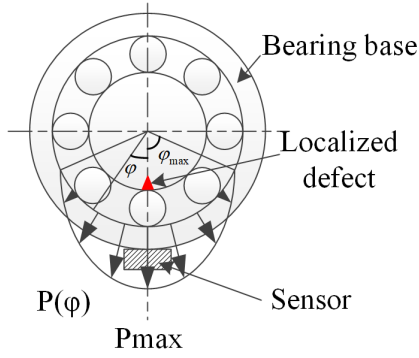


Fig. 1. Nonlinear load distribution under radial load.

expressed as follows:

$$P_{\max} = 1.5 \frac{F}{A} \quad (7)$$

where F represents the pressing force among the mating component with the fault and A represents actual contact area. Considering the incepted defect as a circle of radius “ r ,” the corresponding fault area can be written as πr^2 . Hence, with the increase in the fault size by “ nr ” amount, the area corresponding to the fault increases by “ $n^2 r^2$.” This phenomenon results in the decrease A in (7). As a result, value of “ P_{\max} ” increases swiftly and a low frequency modulation is generated in the signal. With the strengthening of the low frequency modulation, irregularity starts to decrease in the time series and a pattern of regularity starts to form. As a result, SE values are expected to decrease with the progression of fault.

In order to assess the ability of SE in differentiating between outer race and inner race faults in a continuous monitoring process, a synthetic model of bearing fault inception is generated with the help of signals mentioned in (3) and (4). The synthetic model can be expressed by (8) and (9) as follows [6]:

$$X_{\text{Syn}_o}(t) = \begin{cases} \left[\sum_{k=-\alpha}^{\alpha} 5 * \delta(t - kT_0) \right] * e^{-Dt}; & 0.51 < t < 0.61 \\ \left[\sum_{k=-\alpha}^{\alpha} 10 * \delta(t - kT_0) \right] * e^{-Dt}; & 1.12 \leq t \leq 1.22 \\ \left[\sum_{k=-\alpha}^{\alpha} 15 * \delta(t - kT_0) \right] * e^{-Dt}; & 1.74 < t < 1.84 \end{cases} \quad (8)$$

$$X_{\text{Syn}_I}(t) = \begin{cases} \left[\left(\sum_{k=-\infty}^{+\infty} 5 * \delta(t - kT_i) \right) * q(2\pi f_r t) * p(2\pi f_r t) \right] * e^{-Dt}; & 0.51 < t < 0.61 \\ \left[\left(\sum_{k=-\infty}^{+\infty} 10 * \delta(t - kT_i) \right) * q(2\pi f_r t) * p(2\pi f_r t) \right] * e^{-Dt}; & 1.12 \leq t \leq 1.22 \\ \left[\left(\sum_{k=-\infty}^{+\infty} 15 * \delta(t - kT_i) \right) * q(2\pi f_r t) * p(2\pi f_r t) \right] * e^{-Dt}; & 1.74 < t < 1.84. \end{cases} \quad (9)$$

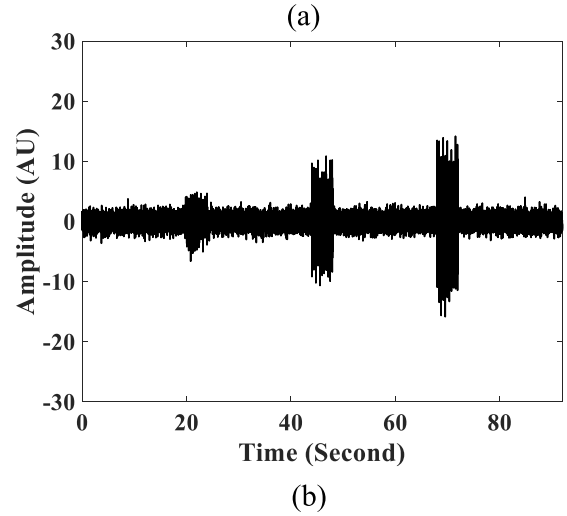
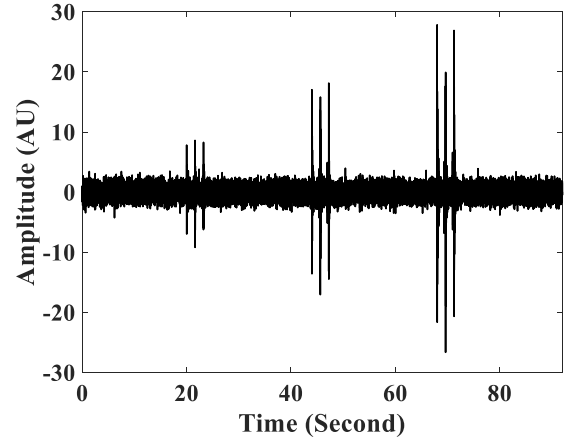


Fig. 2. Synthetic bearing fault model. (a) Outer race fault. (b) Inner race fault.

In the aforementioned discussion, it has been mentioned that SE algorithm cannot differentiate between healthy and faulty conditions under heavy noise; hence, for understanding this weakness, the associated noise level has been kept relatively low (0 dB) with this signal model, as shown in Fig. 2.

A sliding window having data overlapping 75% at a step length of 2 s is used to generate the samples. SE is calculated for both of outer and inner race fault model as shown in Fig. 2 and the calculation result is shown in Fig. 3 as follows.

From Fig. 3, it can be seen that change of SE value with inner and outer race fault follows the same trend toward the downward direction. Hence, it is difficult to distinguish among inner and outer race faults in the continuous monitoring operation by SE.

III. OSCILLATORY SAMPLE ENTROPY

Complete elimination of imbalance and misalignment from a rotor bearing system is a difficult task. Specially, this is more difficult in a large rotating machinery. Hence, the rotating frequency is always present in the vibration data collected from a large rotating machine even if it is operating in a healthy condition. In this context, shaft rotating frequency can be called as PC. Due to the emergence of a fault in

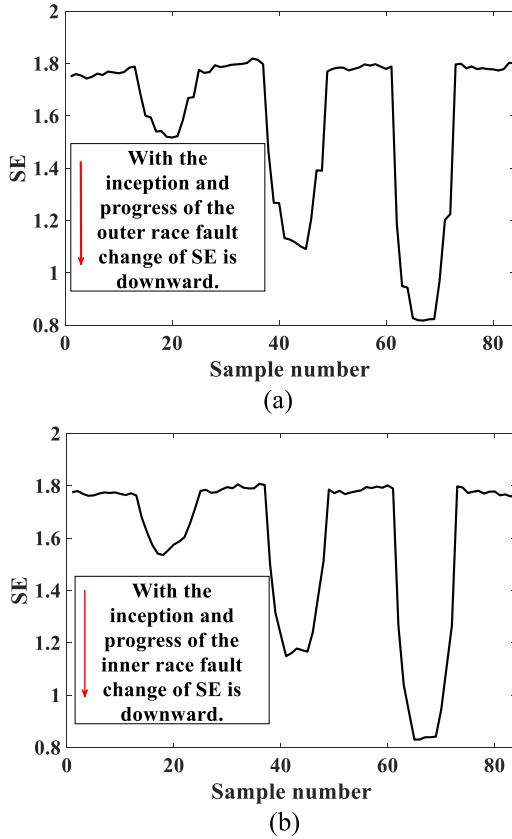


Fig. 3. Change of SE value with (a) outer and (b) inner race fault.

a bearing, corresponding fault-related frequencies are added in it. In addition, the presence of a bearing fault increases the overall vibration of a rotor bearing system, and as a consequence, it also strengthens the bearing PC. As a result, it can be inferred that in terms of energy and amplitude, signal component corresponding to bearing PC is more superior in comparison to the signal component corresponding to bearing fault impulses. In a nutshell, it can be said that bearing PC is the dominating component in a vibration signal collected from rolling element bearing. On the basis of this idea, in this article, instead of applying the original SE algorithm directly on the bearing signal, at first, the relationship between the bearing PC and SE algorithm is found out. Then, oscillatory SE has been calculated with the help of following two phases. In the first phase, signal component corresponding to bearing PC is separated by TQWT. In the following phase, SE algorithm is utilized to quantify the separated bearing PC as a measure of bearing health monitoring.

In the subsections, relationship between bearing PC and SE algorithms, rationale of oscillation-dependent PC separation scheme, theory of oscillation-dependent PC separation, and lastly, calculation procedure of OSE is discussed gradually.

A. Relationship Between Bearing PC and SE Algorithms

In order to study the relationship between bearing PC and SE algorithms, three simulated signals S_1 , S_2 , S_3 have been

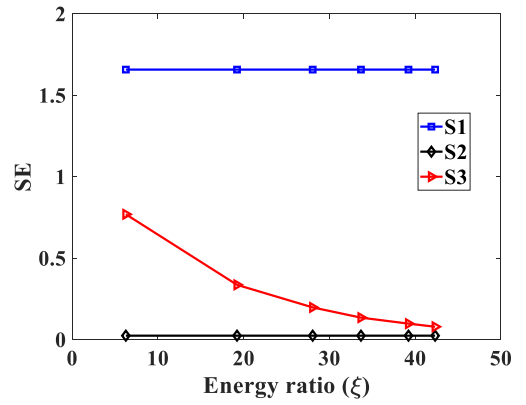


Fig. 4. Biasness of SE toward bearing PC.

generated as follows:

$$S_1(t) = X_o(t) + n(t) \quad (10)$$

$$S_2(t) = \text{Sin}(2\pi f_r t) \quad (11)$$

$$S_3(t) = S_1(t) + S_2(t). \quad (12)$$

In real-life application, bearing fault impulses are associated with noise. Hence, $S_1(t)$ represents the simulated bearing fault impulse $X_o(t)$ with added noise $n(t)$. $n(t)$ is considered Gaussian noise of zero mean and unit variance. $S_2(t)$ represents bearing PC simulated with shaft rotating frequency f_r . $S_3(t)$ represents the summation of $S_1(t)$ and $S_2(t)$. At the beginning, SE values for both $S_1(t)$ and $S_2(t)$ are calculated. Then, by increasing the amplitude of $S_2(t)$, energy ratio between $S_1(t)$ and $S_2(t)$ is gradually increased, and at the same time SE value for the corresponding $S_3(t)$ is calculated. Energy ratio (ξ) between $S_1(t)$ and $S_2(t)$ can be defined as follows:

$$\xi = \log \frac{\|S_2\|_2}{\|S_1\|_2}. \quad (13)$$

Relevant simulation results are shown in Fig. 4.

From Fig. 4, it can be seen that with the increase in the energy and amplitude of the bearing PC, the value of SE of the total signal gets more and more drawn toward it instead of bearing fault impulses. Based on this observation, it can be said that SE is biased toward bearing PC.

On the basis of this finding, it is expected that instead of direct application of SE algorithm on the bearing signal, the SE calculation of bearing PC can provide more efficient results for continuous monitoring of bearing health. Hence, aiming at utilizing the benefits of this finding, in this article, firstly bearing PC is separated from the bearing signal and then its SE value is calculated for performing continuous monitoring of bearing health. Traditional methods, such as wavelet transform or bandpass filters, are not sufficient for separating the PC from a rolling element bearing signal due to their inability to perform efficiently in a continuous monitoring process. Hence, a relatively new method based on TQWT for separating the signal components according to their oscillatory behavior is used in this article. The major advantage of TQWT over traditional methods is the continuously adjustable nature of its parameters

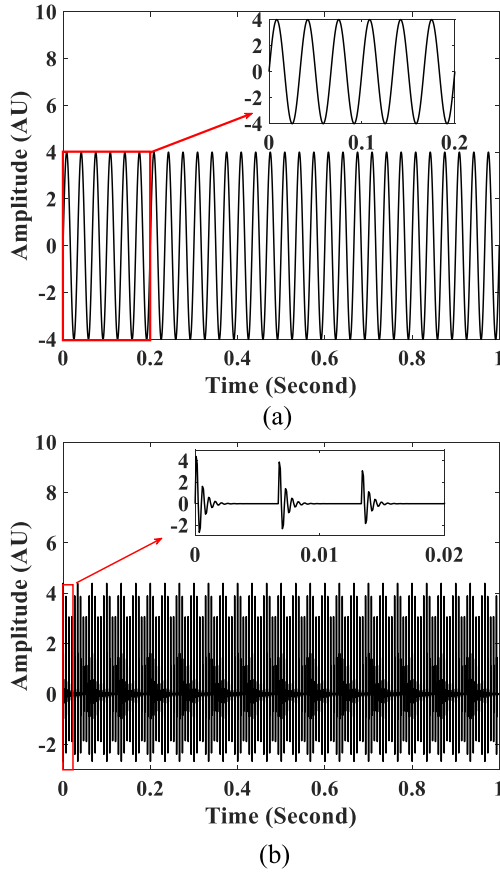


Fig. 5. Simulated key bearing signal components. (a) Bearing PC. (b) Bearing fault impulses.

which makes it suitable for continuous monitoring of bearing health.

B. Rationale of Oscillation-Dependent PC Separation Scheme

A rolling element bearing vibration signal can contain both low oscillatory and high oscillatory signal components. Simulation models have been used to understand this phenomenon. Two key simulated signal components corresponding to bearing PC and fault impulses are shown in Fig. 5.

From Fig. 5, it can be said that a bearing signal component containing the fault impulses can be considered low oscillatory due to exponentially decaying nature of fault impulses while a bearing PC can be considered high oscillatory due to its less spiky continuously oscillating nature. Hence, it is evident that high oscillatory component of a bearing signal can be clearly distinguished from its low oscillatory component. In this context, theoretically, after decomposing by TQWT, bearing PC should lie within high oscillatory component.

As a sparse signal decomposition technique, TQWT is able to separate a signal into its low and high oscillatory components. The decomposition process of TQWT is dependent on Q factor of its wavelet bases which is defined as follows:

$$Q = \frac{F_c}{W} \quad (14)$$

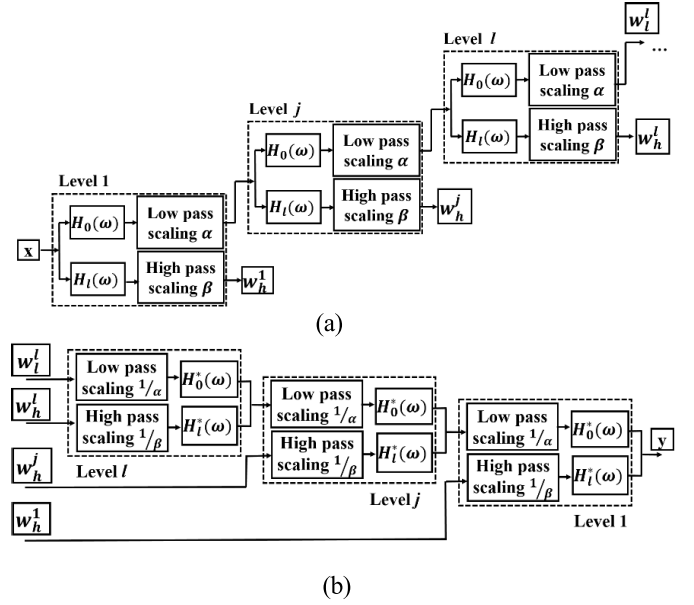


Fig. 6. Dual-channel filters. (a) Decomposition filter. (b) Synthesis filter.

where F_c represents central frequency and W represents pulse bandwidth.

TQWT is applied with the help of a two-channel filter bank. This filter bank is designed by low pass scaling (relevant parameter α) as well as high pass scaling (relevant parameter β). The correlation of α and β can be established with Q factor with the help of another parameter termed as redundancy “ r ” as shown in the following equation:

$$\alpha = 1 - \frac{\beta}{r}, \beta = \frac{2}{Q+1}. \quad (15)$$

Low pass filter $H_0(\omega)$ and high pass filter $H_1(\omega)$ can, respectively, be represented by (16) and (17) as follows:

$$H_0(\omega) = \begin{cases} 1, & |\omega| \leq (1-\beta)\pi \\ \theta\left(\frac{\omega + (\beta-1)\pi}{\alpha + \beta - 1}\right), & (1-\beta)\pi \leq \omega \leq \alpha\pi \\ 0, & \alpha\pi \leq |\omega| \leq \pi \end{cases} \quad (16)$$

$$H_1(\omega) = \begin{cases} 0, & |\omega| \leq (1-\beta)\pi \\ \theta\left(\frac{\alpha\pi - \omega}{\alpha + \beta - 1}\right), & (1-\beta)\pi \leq \omega \leq \alpha\pi \\ 1, & \alpha\pi \leq |\omega| \leq \pi \end{cases} \quad (17)$$

where θ infers a function such as $\theta(v) = 0.5(1 + \cos v)(2 - \cos v)^{1/2}$, $|v| < \pi$. Equations (15)–(17) can be used to parametrize TQWT with the help of Q factor and redundancy r . Fig. 6 shows the application of TQWT with the help of two channel filter bank.

The maximum possible decomposition level number, L_{\max} , can be calculated by (18) [27] as follows:

$$L_{\max} = \left\lfloor \frac{\log(N/4(Q+1))}{\log((Q+1)/((Q+1) - \frac{2}{r}))} \right\rfloor \quad (18)$$

where $\lfloor \cdot \rfloor$ infers a rounding operation and the number of data points are represented by N . “ $L+1$ ” number of subbands are generated after applying an “ L ” stage decomposition.

Given a bearing signal “ x_{bearing}^R ” comprised of both high oscillatory component “ $x_{h(\text{bearing})}^R$ ” and low oscillatory component “ $x_{l(\text{bearing})}^R$ ” such as

$$x_{\text{bearing}}^R = x_{h(\text{bearing})}^R + x_{l(\text{bearing})}^R. \quad (19)$$

In this research, it is aimed to decompose x_{bearing}^R into $x_{h(\text{bearing})}^R$ and $x_{l(\text{bearing})}^R$, respectively, by morphological component analysis (MCA) [40].

Given that Q_l factor corresponding to low oscillatory component (Q_l) and Q_h factor corresponding to high oscillatory component (Q_h) are to be utilized for two different TQWTs named TQWT1 and TQWT2, respectively, (20) gives the aimed decomposition with the help of a constrained optimization method as follows:

$$\begin{cases} \arg_{w_1, w_2} \min \sum_{j=1}^{j_1+1} \lambda_{1j} \|w_{1j}\|_1 + \sum_{j=1}^{j_2+1} \lambda_{2j} \|w_{2j}\|_1 \\ x_{\text{bearing}}^R = \text{TQWT1}^{-1}(w_1) + \text{TQWT2}^{-1}(w_2) \end{cases} \quad (20)$$

where λ_1 and λ_2 are regularization parameter and subsidiary bands of TQWT_i ($i = 1, 2$) are represented by w_{ij} .

After obtaining the values of w_1 and w_2 , we can find $x_{h(\text{bearing})}^R$ and $x_{l(\text{bearing})}^R$ as follows:

$$\begin{cases} x_{h(\text{bearing})}^R = \text{TQWT1}^{-1}(w_1) \\ x_{l(\text{bearing})}^R = \text{TQWT2}^{-1}(w_2). \end{cases} \quad (21)$$

In real industrial application, bearing signals are associated with random noise present in the surrounding environment. Hence, (19) can be written as follows:

$$x_{\text{bearing}}^R = x_{h(\text{bearing})}^R + x_{l(\text{bearing})}^R + \text{noise}. \quad (22)$$

Equation (23) is used for solving the stated problem

$$\arg_{w_1, w_2} \min \|x_{\text{bearing}}^R - \varphi_1 w_1 - \varphi_2 w_2\| + \sum_{j=1}^{j_1+1} \lambda_{1j} \|w_{1j}\|_1 + \sum_{j=1}^{j_2+1} \lambda_{2j} \|w_{2j}\|_1 \quad (23)$$

where inverse TQWT is represented by φ_1 and φ_2 , respectively. Power of the signals can be used to determine the values of λ_1 and λ_2 [29].

C. OSE Calculation for Continuous Monitoring of Rolling Element Bearing Health

Continuous health monitoring of a bearing infers that the vibration responses are recorded at a specific time interval and each recording is investigated at a time when the total monitoring work is achieved by adding the subsequent analysis result altogether. In this context, referring to the original definition of SE, OSE can be calculated using following steps:

Step 1: For a particular time point R , a signal x_{bearing}^R is obtained from a rolling element bearing. R can be defined as follows:

$$R = R_0 + \Delta r \quad (24)$$

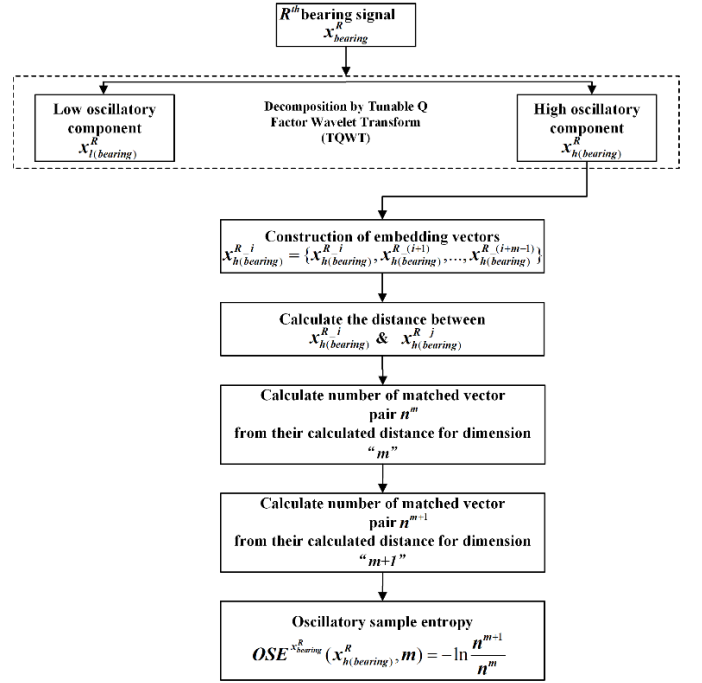


Fig. 7. Framework of OSE calculation.

where R_0 represents the beginning moment of data collection and Δr represents the constant time delay between each recording.

Step 2: The high oscillatory component $x_{h(\text{bearing})}^R$ is extracted from x_{bearing}^R .

Step 3: Following Taken’s embedding theorem, embedding vectors from $x_{h(\text{bearing})}^R$ with dimension m are constructed as follows:

$$x_{h(\text{bearing})}^{R,i} = \{x_{h(\text{bearing})}^{R,i}, x_{h(\text{bearing})}^{R,i+1}, \dots, x_{h(\text{bearing})}^{R,i+m-1}\}, \quad 1 \leq i \leq N - m \quad (25)$$

where “ N ” is the length of separated $x_{h(\text{bearing})}^R$.

Step 4: If two vectors $x_{h(\text{bearing})}^{R,i}$ and $x_{h(\text{bearing})}^{R,j}$ are equal where $i \neq j$, then $\{x_{h(\text{bearing})}^{R,i}, x_{h(\text{bearing})}^{R,j}\}$ can be called as an “ m ” dimensional matched pair vector. Let us consider that n^m represents the total number of “ m ”-dimensional matched vector pairs.

Step 5: Steps 3 and 4 are repeated for dimension “ $m = m + 1$ ” and then “ n^{m+1} ” number of matched vector pairs are obtained for dimension “ $m + 1$.”

Step 6: OSE for x_{bearing}^R , $\text{OSE}^{x_{\text{bearing}}^R}$ is calculated by the ratio of “ n^{m+1} ” to “ n^m ” as follows:

$$\text{OSE}^{x_{\text{bearing}}^R}(x_{h(\text{bearing})}^R, m) = -\ln \frac{n^{m+1}}{n^m}. \quad (26)$$



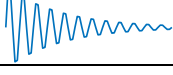
Fig. 7 shows the flowchart for calculating the OSE.

IV. PARAMETER SELECTION OF OSE

A. Parameters Related to TQWT

Calculation of OSE is dependent on three parameters related to TQWT [33]. The TQWT-related parameters are “ Q ,” “ r ,” and “ L_{max} .” As described in Section III-B, “ Q ” represents

TABLE II
VALUES OF DIFFERENT SPARSITY INDICES UNDER VARYING
OSCILLATORY CONDITIONS

Signal	K	NE	RSI	GI
	32.730	2.583	267.56	0.924
	16.475	1.9902	87.6705	0.8512
	8.2594	1.3419	10.5409	0.7112

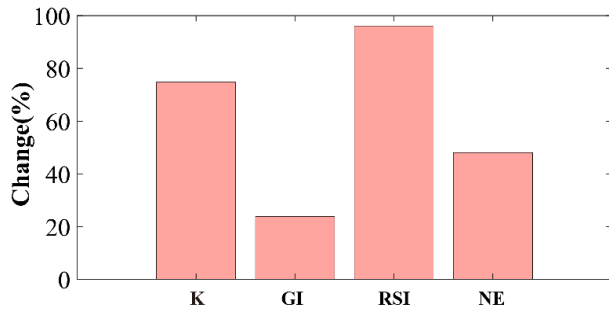


Fig. 8. Sensitiveness of sparsity indices toward the oscillatory nature of bearing signal.

the oscillation level of the signal component, “ r ” represents the redundancy, and “ L_{\max} ” represents the number of decomposition level. Among the three parameters described above, “ r ” and “ L ” can be chosen from literature. In real-life practical situation, “ r ” is suggested to choose more than 1. However, a higher value of “ r ” will increase the computational cost [41], [42]. Considering these, the value of “ r ” in this article is chosen as 3. Also, “ L_{\max} ” is calculated by (18) [27].

Two most important parameters corresponding to the TQWT-based decompositions are the Q factors [43]. Considering the transient nature of bearing fault impulses value of low Q factor, “ Q_1 ” should be as small as possible. Since “ Q_1 ” cannot be less than 1, in this research, the value of “ Q_1 ” is selected as 1. However, the selection of high Q factor “ Q_h ” is a data-dependent criterion. Hence, it is required to achieve suitable optimization for that. Considering the ability of sparsity indices in quantifying the peakedness corresponding to the low oscillatory and high oscillatory signal components, they are a suitable criterion for achieving the aforementioned decomposition [44], [45]. As a result, aiming at selecting the suitable “ Q_h ,” an optimization study among signals of varying oscillatory level has been conducted with the help of representative sparsity indices such as kurtosis (K), negative entropy (NE), reciprocal smoothness index (RSI), and gini index (GI). The use of sparsity indices for optimization purpose is motivated by their ability to characterize the impulsiveness of a signal [46], [47]. The lower the impulsiveness of a signal, the higher oscillation level it possesses and vice versa [48]. Table II represents the values of different sparsity indices under different oscillation levels.

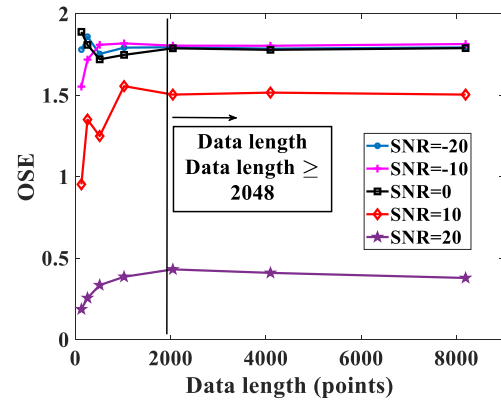


Fig. 9. Relationship of data length with OSE calculation.

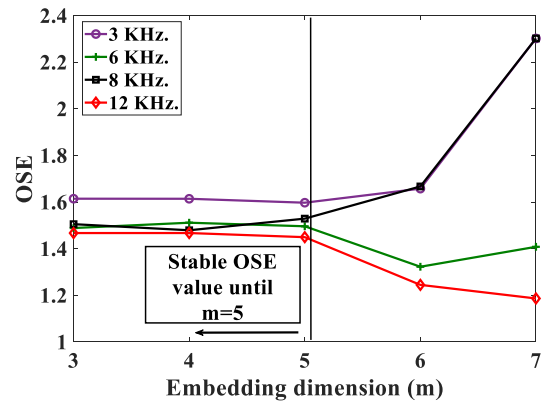


Fig. 10. Effect of the embedding dimension (m) on the calculation of OSE.

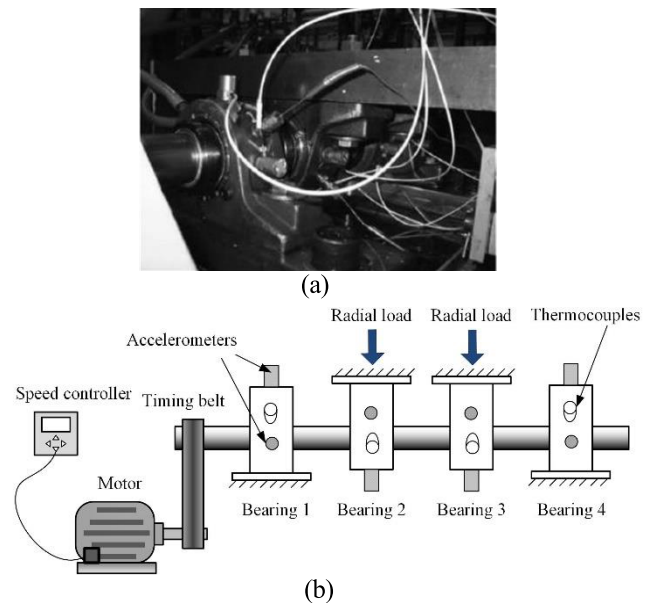


Fig. 11. Experimental equipment and schematic of the experimental setup for the IMS data. (a) Experimental equipment. (b) Sketch of bearing-accelerated life testing system.

From Table II, it can be seen that with the gradual progression from low oscillatory to high oscillatory behavior, values of the corresponding sparsity indices decrease. Hence,

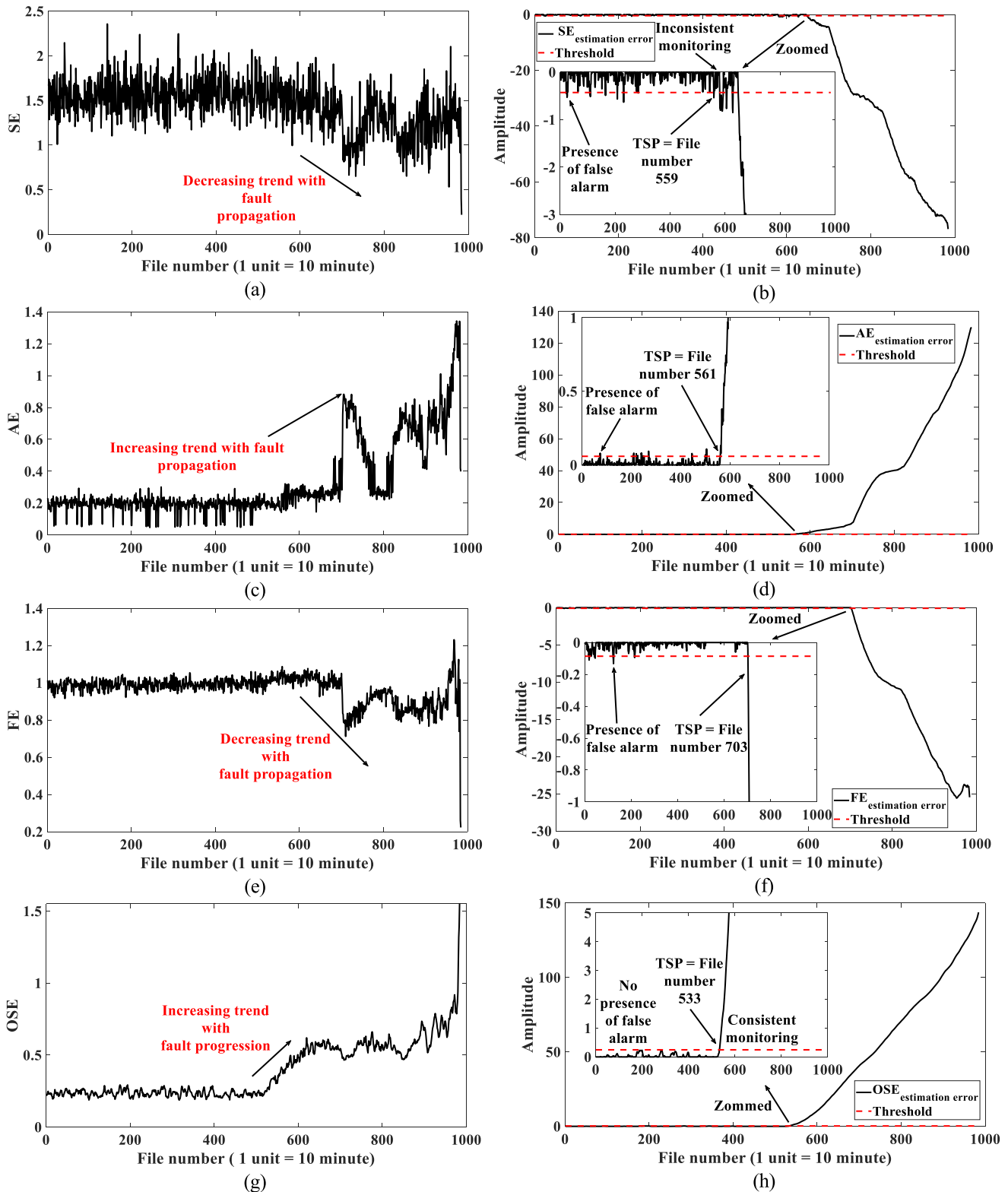


Fig. 12. Complete life of analyzed bearing by different entropy-based indices. (a) Change of SE values. (b) Monitoring based on (a). (c) Change of AE values. (d) Monitoring based on (c). (e) Change of FE values. (f) Monitoring based on (e). (g) Change of OSE values. (h) Monitoring based on (g).

for comparison purpose among the sparsity indices, the rate of decrease of different sparsity indices while shifting from lowest oscillatory to the highest oscillatory, as shown in Table II, is calculated and shown in Fig. 8.

It can be seen from Fig. 8 that rate of change of RSI with that of oscillatory nature of the bearing signal is the highest compared to other sparsity indices. Hence, in this research, RSI is used to perform the optimized selection

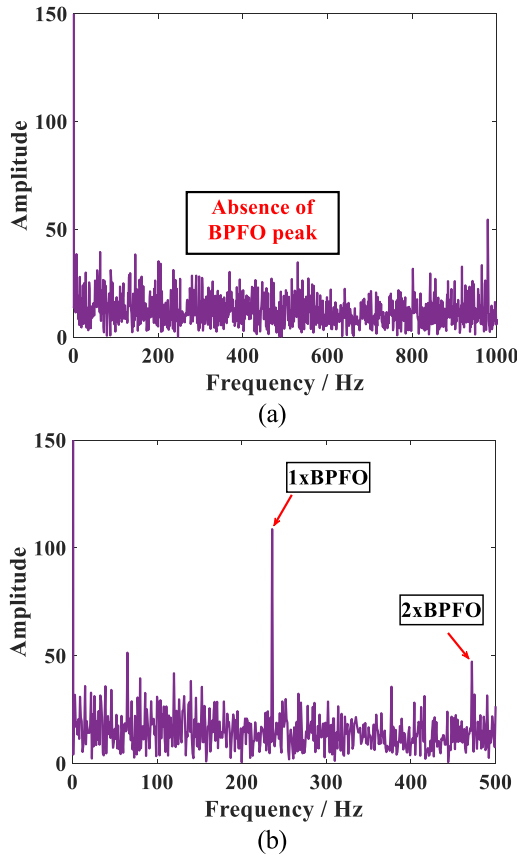


Fig. 13. Envelope spectrum at key files. (a) 200th file. (b) 533rd file.

of high oscillatory component “ Q_h ” with the help of the following equation:

$$Q_h = \arg_{Q_h} \min \text{RSI}(Q_h). \quad (27)$$

The iteration range for Q_h is selected as in [4] and [12], with an increment rate of each step being 0.5 [29], [47].

B. Data Length Selection

Considering the effect of data length on the SE, in this section, a study has been conducted under the influence of different noise levels regarding the selection of data length in OSE calculation. The fault signal simulated by (3) is used for this purpose. The result regarding the selection of data length with OSE calculation is shown in Fig. 9.

From Fig. 9, when the value of the data length is ≥ 2048 , the proposed OSE becomes relatively stable under different levels of noise. Considering the relationship between the computational cost with the data length, in this research, 2048 is utilized as the length of vibration recordings.

C. Selection of the Embedding Dimension (m)

As described in (24), the value of OSE is dependent on the value of embedding dimension (m). Hence, in this section, a study has been conducted regarding the selection of suitable value of embedding dimension (m). For the chosen data length 2048, as discussed in Section IV-B, OSE value is calculated for

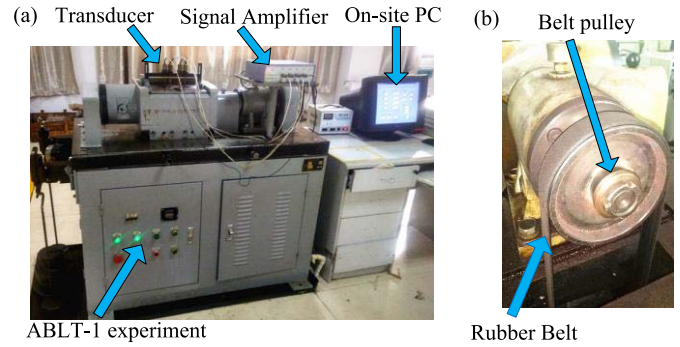


Fig. 14. (a) Experiment equipment. (b) Rubber belt.

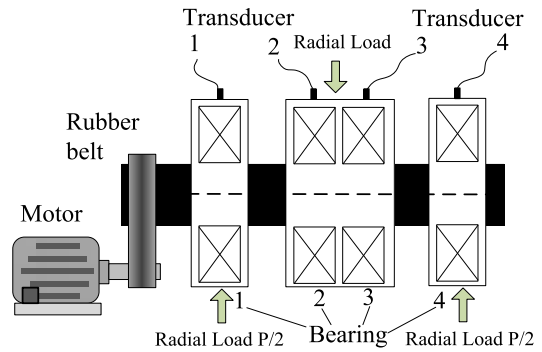


Fig. 15. Sketch of bearing-accelerated life test system.

the signal simulated by (3) under different sampling frequency, as shown in Fig. 10.

From Fig. 10, it can be found that values for OSE under different sampling rates are stable until $m = 5$. With the increase in m -value > 5 , the values of OSE under different sampling rates become more and more scattered. This phenomenon may be caused by the occurrence of information loss due to the increase in the embedding dimension (m) as discussed in [49] and [50]. Moreover, very large value of “ m ” is also unfavorable in regards to computational complexity. Additionally, a too large value of “ m ” will require a very long time series which is difficult in practical application. Considering all these aspects, in this article, embedding dimension “ m ” is chosen as 5.

V. EXPERIMENTAL VERIFICATION

Two different experimental studies are utilized to verify the performance of the proposed OSE. Performance of the proposed OSE has been compared with SE, approximate entropy (AE), and fuzzy entropy (FE).

A. Experimental Case Study-1

In order to verify the effectiveness of the proposed OSE, bearing run to failure experimental data from Center for Intelligent Maintenance Systems (IMS), University of Cincinnati, was used [51]. A schematic of the experimental setup for the data collection is shown in Fig. 11.

In this experiment, four Rexnord ZA-2115 bearings are mounted on the support shaft. Data were collected at a rotating speed of 2000 rpm. Bearings were kept lubricated using the

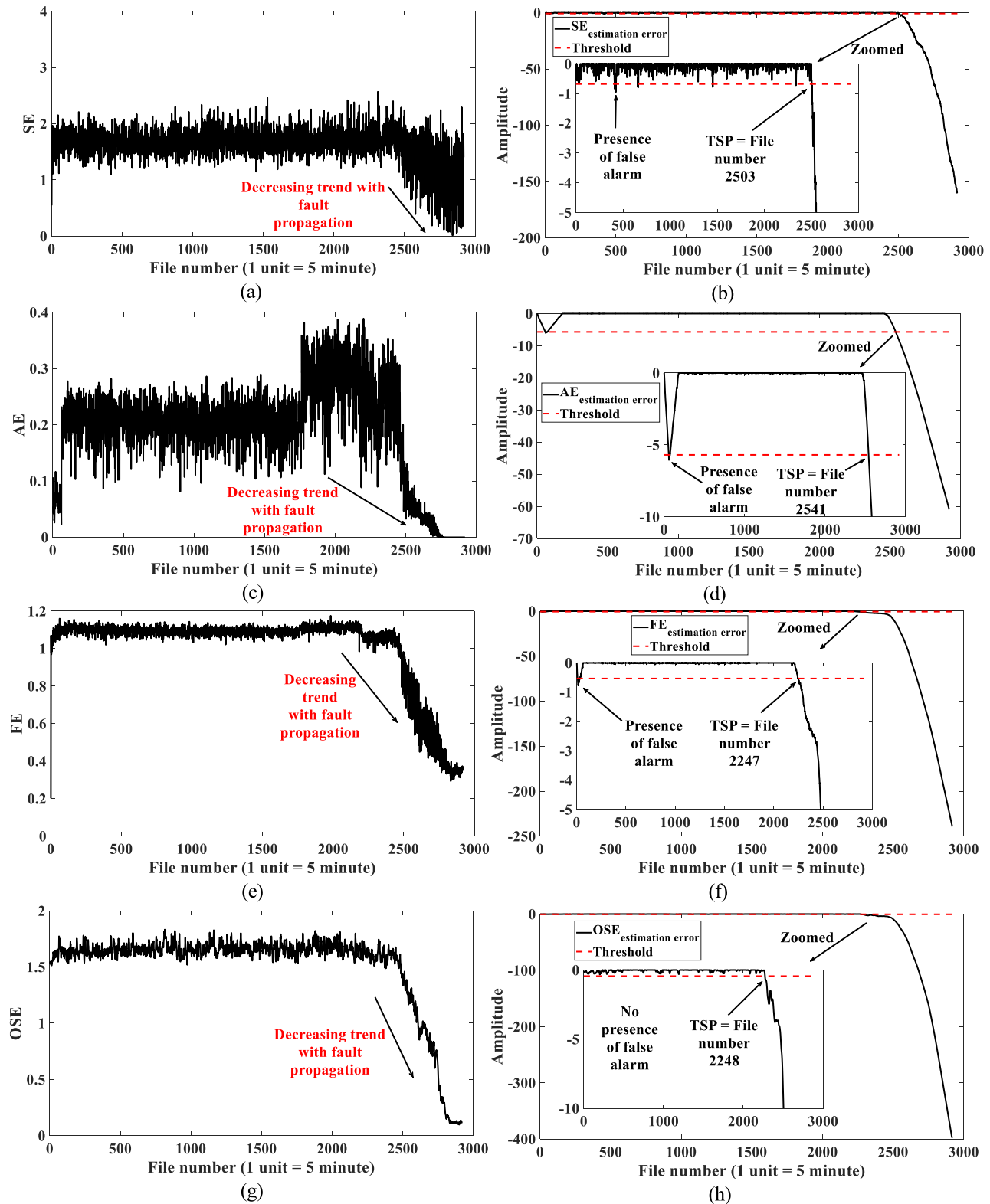


Fig. 16. Complete life of analyzed bearing by different entropy-based indices. (a) Change of SE values. (b) Monitoring based on (a). (c) Change of AE values. (d) Monitoring based on (c). (e) Change of FE values. (f) Monitoring based on (e). (g) Change of OSE values. (h) Monitoring based on (g).

force mechanism. A radial load of 6000 lbs was used on the bearings. Sampling frequency of the data collection was kept at 20 480 Hz. Data are collected at an interval of 10 min between each recording. The magnetic plug was used to

collect the debris from the oil. When the amount of debris crosses a certain limit, the test is stopped and the bearing is observed. A total of 984 recording files were collected. Upon the inspection of the bearing at the end of data collection,

an outer race fault is found. Four indices, i.e., SE, AE, FE, and OSE, as described before have been used to monitor the health of the bearing by collected vibration data.

It is assumed that bearing runs in a normal condition from file number 1 to file number 200. Based on this, the threshold for monitoring the bearing health is designed by cumulative sum (CUSUM)-based processing of the estimation error [52], [53]. With the help of the CUSUM method, the deviation of monitored value is accumulated from the set point of control variable for all samples. Change of different indices and their corresponding CUSUM-based monitoring result is shown in Fig. 12.

From Fig. 12, it can be seen that time to start point (TSP) of the fault for SE, AE, FE, and OSE are, respectively, at file numbers 559, 561, 703, and 533, respectively. In order to study the effectiveness of the proposed OSE, envelope spectrum analysis has been carried out at file number 533. Additionally, in order to confirm the design of threshold, envelope spectrum analysis has been carried out at file number 200. According to the bearing specification presented with the data file, ball passing frequency for outer race fault (BPFO) is 236 Hz. The result of the envelope spectrum is shown in Fig. 13.

From Fig. 13, it can be seen that envelope spectrum at file number 533 contains the BPFO peak. However, no BPFO peak is located in the envelope spectrum of file number 200. This infers that designing of the threshold is correct and OSE can detect the fault accurately. Considering the irreversible nature of bearing health degradation, it can be said that OSE detects the presence of faults 260, 280, and 1700 min earlier than SE, AE, and FE, respectively. Moreover, it can be seen that values of SE and FE decreases with the propagation of the fault which is contradictory to the theoretical concept discussed in Section II-B. In this context, both OSE and AE demonstrate the expected trend with the progression of fault. However, similar to SE and FE, values of AE also provide false alarm. On the contrary, OSE demonstrates consistent monitoring results all along the monitoring period.

B. Experimental Case Study-2

Accelerated bearing life test (ABLT-1) data for experimental case study-2 have been collected from Hangzhou Bearing Test and Research Center (HBRC), China. The set up for the experiment is shown in Fig. 14.

The experimental setup consists of four bearings mounted on a shaft. The shaft is driven by an ac motor. As shown in Fig. 14(b), the ac motor and the shaft are connected by a rubber belt using two belt pulleys. Transmission cost and generated noise are less in a setup run by rubber belt. Diameter of both of the belt pulleys are 134 mm. A schematic of the bearing-accelerated run to failure life test setup is shown in Fig. 15.

The bearing model used in this experiment is the single-row deep-groove ball bearings. Each bearing consists of eight balls with a 0° contact angle. Pitch diameter of the bearing is 65.5 mm, while the corresponding ball diameter is 15.081 mm. The outer race of the bearing is fixed and the inner race rotates with the shaft. Upon failure of a bearing, it was replaced

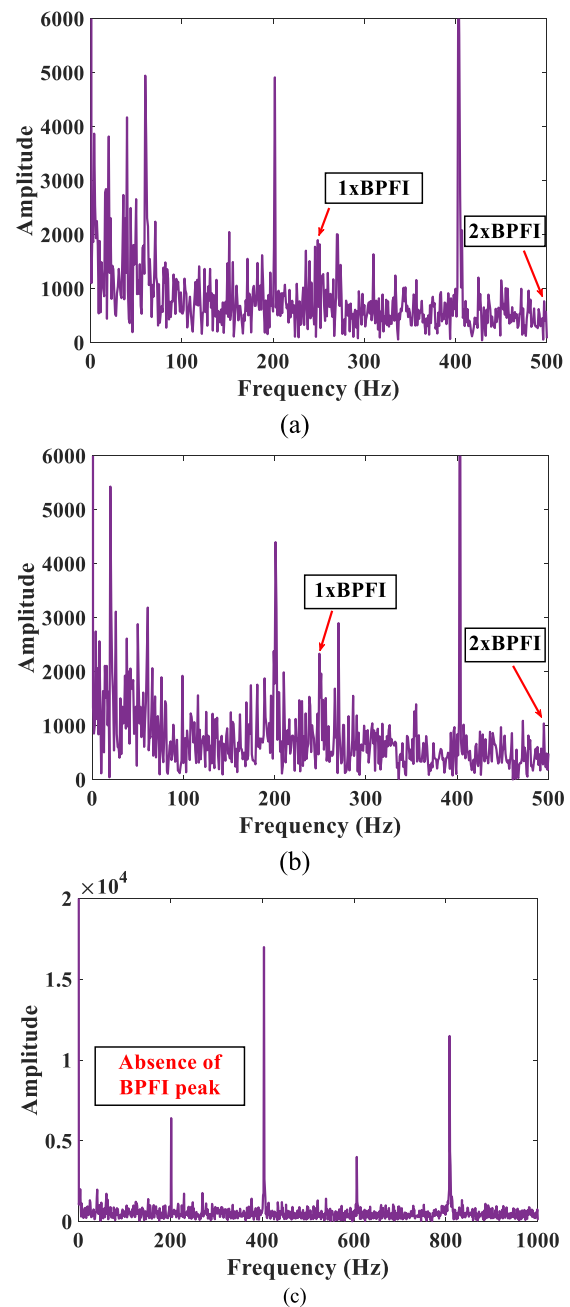


Fig. 17. Envelope spectrum analysis at key files. (a) 2247th file. (b) 2248th file. (c) 500th file.

by another one. Rotational speed of the bearing is kept at 3000 rpm. A radial load of 20.5 kg was applied initially which was amplified by 100 times by oil pressure amplifying unit. A force oil-based lubrication system was used to control the temperature at or around 58°C . Four accelerometers are shown in Fig. 15. The transducers were set on the bearing housing for data collection. Data are collected at an interval of 5 min. The data were recorded at a sampling frequency of 20 480 Hz. At the end of run to failure test, an inner race fault is found on the analyzed bearing.

SE, AE, FE, and OSE are utilized to interpret the whole life cycle of the analyzed bearing. In this experiment, the first

500 samples have been considered as the normal health state to build the CUSUM-based monitoring model and calculate the fault threshold value. From Fig. 16, it can be seen that TSP for SE, AE, FE, and OSE are, respectively, 2503, 2541, 2248, and 2250. The envelope spectra at file numbers 2248 and 2250 have been conducted to understand the accuracy of the fault detection. Also, to validate the designing of the threshold value, envelope spectrum analysis has been conducted for file number 500. According to bearing specification, the ball passing frequency for inner race fault (BPFI) is 246 Hz. The result of envelope spectrum is shown in Fig. 17.

From Fig. 17, it can be seen that all the key files contain peaks at BPFI. This implies that FE and OSE both can detect fault correctly. However, like SE and AE, FE also provides false alarm. Additionally, since no fault has been found at file number 500, bearing health before the file number 500 can be considered normal. In this context, OSE shows consistent monitoring performance throughout the whole monitoring phase without the presence of any false alarm and detects the fault earlier in compare to original SE and AE.

Additionally, change of SE and FE values with propagation of inner race fault is downward which is similar to that of outer race fault for SE and FE shown in Section V-A. However, change of OSE with the inner race fault progression is downward which is different from that of that outer race fault (upward) as shown in Section V-A. Hence, it can be said that by observing the change of OSE value it will be possible to distinguish between outer and inner race faults.

VI. CONCLUSION

Focusing on the limitations of SE in continuous monitoring of rolling element bearing health, an OSE is proposed in this article. The major novelties of this study fall into two aspects. Firstly, biasness of SE algorithm toward the bearing PC is found out. Secondly, PC of bearing signal is separated with the help of continuously adjustable TQWT. The proposed OSE solves the weaknesses of original SE algorithm by not only detecting bearing fault at an earlier time of inception but also accurately differentiating between inner and outer race faults by showing the expected degradation trend according to theoretical analysis. Two case studies are performed to validate the superiority of OSE with the state of the art SE, AE, and FE methods. Experimental results demonstrate that the proposed OSE is better in terms of early detection of bearing fault, consistent monitoring of bearing health and automatic identification of inner and outer race faults.

It is possible to address the nonlinearity and nonstationarity associated with bearing vibration signal with the help of the proposed OSE. As a result, it can be a promising tool for the researchers especially in the areas of artificial neural network, remaining useful life, and so on.

REFERENCES

[1] M. Cerrada *et al.*, "A review on data-driven fault severity assessment in rolling bearings," *Mech. Syst. Signal Process.*, vol. 99, pp. 169–196, Jan. 2018.
 [2] D. Wang and K. Tsui, "Statistical modeling of bearing degradation signals," *IEEE Trans. Rel.*, vol. 66, no. 4, pp. 1331–1344, Dec. 2017.

[3] W. Qian and S. Li, "A novel class imbalance-robust network for bearing fault diagnosis utilizing raw vibration signals," *Measurement*, vol. 156, May 2020, Art. no. 107567.
 [4] B. Hou, D. Wang, Y. Wang, T. Yan, Z. Peng, and K.-L. Tsui, "Adaptive weighted signal preprocessing technique for machine health monitoring," *IEEE Trans. Instrum. Meas.*, vol. 70, pp. 1–11, 2021.
 [5] S. Sheng, L. Zhang, and R. X. Gao, "A systematic sensor-placement strategy for enhanced defect detection in rolling bearings," *IEEE Sensors J.*, vol. 6, no. 5, pp. 1346–1354, Oct. 2006.
 [6] Y. Li, F. Liu, S. Wang, and J. Yin, "Multiscale symbolic Lempel–Ziv: An effective feature extraction approach for fault diagnosis of railway vehicle systems," *IEEE Trans. Ind. Informat.*, vol. 17, no. 1, pp. 199–208, Jan. 2021.
 [7] G. Qingjun and L. Yang, "Early fault diagnosis of rolling bearing based on Lyapunov exponent," *J. Phys., Conf. Ser.*, vol. 1187, no. 3, Apr. 2019, Art. no. 032073.
 [8] D. Wang, J. Zhong, C. Shen, E. Pan, Z. Peng, and C. Li, "Correlation dimension and approximate entropy for machine condition monitoring: Revisited," *Mech. Syst. Signal Process.*, vol. 152, May 2021, Art. no. 107497.
 [9] C. Dou and J. Lin, "Adaptive multiscale symbolic-dynamics entropy for condition monitoring of rotating machinery," *Entropy*, vol. 21, no. 12, p. 1138, Nov. 2019.
 [10] R. Yan and R. X. Gao, "Approximate entropy as a diagnostic tool for machine health monitoring," *Mech. Syst. Signal Process.*, vol. 21, no. 2, pp. 824–839, Feb. 2007.
 [11] Y. Li, X. Wang, Z. Liu, X. Liang, and S. Si, "The entropy algorithm and its variants in the fault diagnosis of rotating machinery: A review," *IEEE Access*, vol. 6, pp. 66723–66741, 2018.
 [12] C. E. Shannon, "A mathematical theory of communication," *Bell Syst. Tech. J.*, vol. 27, no. 3, pp. 379–423, Jul. 1948.
 [13] J. S. Richman and J. R. Moorman, "Physiological time-series analysis using approximate entropy and sample entropy," *Amer. J. Physiol.-Heart Circulatory Physiol.*, vol. 278, no. 6, pp. H2039–H2049, Jun. 2000.
 [14] C. Bandt and B. Pompe, "Permutation entropy: A natural complexity measure for time series," *Phys. Rev. Lett.*, vol. 88, Apr. 2002, Art. no. 174102.
 [15] L. Zhang, G. Xiong, H. Liu, H. Zou, and W. Guo, "An intelligent fault diagnosis method based on multiscale entropy and SVMs," in *Proc. Int. Symp. Neural Netw.*, 2009, pp. 724–732.
 [16] P. Bangalore and L. B. Tjernberg, "An artificial neural network approach for early fault detection of gearbox bearings," *IEEE Trans. Smart Grid*, vol. 6, no. 2, pp. 980–987, Mar. 2015.
 [17] H. Wang, H. Wang, G. Jiang, J. li, and Y. Wang, "Early fault detection of wind turbines based on operational condition clustering and optimized deep belief network modeling," *Energies*, vol. 12, no. 6, p. 984, 2019.
 [18] J. Liang, J.-H. Zhong, and Z.-X. Yang, "Correlated EEMD and effective feature extraction for both periodic and irregular faults diagnosis in rotating machinery," *Energies*, vol. 10, no. 10, p. 1652, Oct. 2017.
 [19] L. Zhang, G. Xiong, H. Liu, H. Zou, and W. Guo, "Fault diagnosis based on optimized node entropy using lifting wavelet packet transform and genetic algorithms," *Proc. Inst. Mech. Eng., I, J. Syst. Control Eng.*, vol. 224, no. 5, pp. 557–573, Aug. 2010.
 [20] M. Seera, M. L. D. Wong, and A. K. Nandi, "Classification of ball bearing faults using a hybrid intelligent model," *Appl. Soft Comput.*, vol. 57, pp. 427–435, Aug. 2017.
 [21] K. Noman, Q. He, Z. Peng, and D. Wang, "A scale independent flexible bearing health monitoring index based on time frequency manifold energy & entropy," *Meas. Sci. Technol.*, vol. 31, no. 11, Nov. 2020, Art. no. 114003.
 [22] Y. Lei, J. Lin, Z. He, and M. J. Zuo, "A review on empirical mode decomposition in fault diagnosis of rotating machinery," *Mech. Syst. Signal Process.*, vol. 35, nos. 1–2, pp. 108–126, Feb. 2013.
 [23] Y. Li, S. Si, Z. Liu, and X. Liang, "Review of local mean decomposition and its application in fault diagnosis of rotating machinery," *J. Syst. Eng. Electron.*, vol. 30, pp. 799–814, Aug. 2019.
 [24] H. Han, S. Cho, S. Kwon, and S.-B. Cho, "Fault diagnosis using improved complete ensemble empirical mode decomposition with adaptive noise and power-based intrinsic mode function selection algorithm," *Electronics*, vol. 7, no. 2, p. 16, Jan. 2018.
 [25] J. Wang, G. Du, Z. Zhu, C. Shen, and Q. He, "Fault diagnosis of rotating machines based on the EMD manifold," *Mech. Syst. Signal Process.*, vol. 135, Jan. 2020, Art. no. 106443.
 [26] Z. Wu and N. E. Huang, "Ensemble empirical mode decomposition: A noise-assisted data analysis method," *Adv. Adapt. Data Anal.*, vol. 1, no. 1, pp. 1–41, 2009.

- [27] I. W. Selesnick, "Wavelet transform with tunable Q-factor," *IEEE Trans. Signal Process.*, vol. 59, no. 8, pp. 3560–3575, Aug. 2011.
- [28] J. Luo, D. Yu, and M. Liang, "A kurtosis-guided adaptive demodulation technique for bearing fault detection based on tunable-Q wavelet transform," *Meas. Sci. Technol.*, vol. 24, no. 5, May 2013, Art. no. 055009.
- [29] Y. Li, X. Liang, M. Xu, and W. Huang, "Early fault feature extraction of rolling bearing based on ICD and tunable Q-factor wavelet transform," *Mech. Syst. Signal Process.*, vol. 86, pp. 204–223, Mar. 2017.
- [30] B. Chen *et al.*, "Fault diagnosis method based on integration of RSSD and wavelet transform to rolling bearing," *Measurement*, vol. 131, pp. 400–411, Jan. 2019.
- [31] Y. Hu, Q. Zhou, J. Gao, J. Li, and Y. Xu, "Compound fault diagnosis of rolling bearings based on improved tunable Q-factor wavelet transform," *Meas. Sci. Technol.*, vol. 32, no. 10, Oct. 2021, Art. no. 105018.
- [32] J. Ding, J. Zhou, and Y. Yin, "Fault detection and diagnosis of a wheelset-bearing system using a multi-Q-factor and multi-level tunable Q-factor wavelet transform," *Measurement*, vol. 143, pp. 112–124, Sep. 2019.
- [33] P. Ma, H. Zhang, W. Fan, and C. Wang, "Early fault diagnosis of bearing based on frequency band extraction and improved tunable Q-factor wavelet transform," *Measurement*, vol. 137, pp. 189–202, Apr. 2019.
- [34] H. Wang, J. Chen, and G. Dong, "Feature extraction of rolling bearing's early weak fault based on EEMD and tunable Q-factor wavelet transform," *Mech. Syst. Signal Process.*, vol. 48, nos. 1–2, pp. 103–119, Oct. 2014.
- [35] P. D. McFadden and J. D. Smith, "Model for the vibration produced by a single point defect in a rolling element bearing," *J. Sound Vib.*, vol. 96, no. 1, pp. 69–82, Sep. 1984.
- [36] S.-D. Wu, C.-W. Wu, S.-G. Lin, K.-Y. Lee, and C.-K. Peng, "Analysis of complex time series using refined composite multiscale entropy," *Phys. Lett. A*, vol. 378, no. 20, pp. 1369–1374, Apr. 2014.
- [37] R. Yan and R. X. Gao, "Complexity as a measure for machine health evaluation," *IEEE Trans. Instrum. Meas.*, vol. 53, no. 4, pp. 1327–1334, Aug. 2004.
- [38] R. Yan, Y. Liu, and R. X. Gao, "Permutation entropy: A nonlinear statistical measure for status characterization of rotary machines," *Mech. Syst. Signal Process.*, vol. 29, pp. 474–484, May 2012.
- [39] R. B. Randall, "A new method of modeling gear faults," *J. Mech. Des.*, vol. 104, no. 2, pp. 259–267, Apr. 1982.
- [40] J.-L. Starck, M. Elad, and D. L. Donoho, "Image decomposition via the combination of sparse representations and a variational approach," *IEEE Trans. Image Process.*, vol. 14, no. 10, pp. 1570–1582, Oct. 2005.
- [41] I. W. Selesnick, "Sparse signal representations using the tunable Q-factor wavelet transform," *Proc. SPIE*, vol. 81381U, Sep. 2011, Art. no. 81381U.
- [42] G. Cai, X. Chen, and Z. He, "Sparsity-enabled signal decomposition using tunable Q-factor wavelet transform for fault feature extraction of gearbox," *Mech. Syst. Signal Process.*, vol. 41, nos. 1–2, pp. 34–53, Dec. 2013.
- [43] X. Chen, G. Cai, H. Cao, and W. Xin, "Condition assessment for automatic tool changer based on sparsity-enabled signal decomposition method," *Mechatronics*, vol. 31, pp. 50–59, Oct. 2015.
- [44] Y. Miao, M. Zhao, and J. Hua, "Research on sparsity indexes for fault diagnosis of rotating machinery," *Measurement*, vol. 158, Jul. 2020, Art. no. 107733.
- [45] B. Hou, D. Wang, T. Yan, Y. Wang, Z. Peng, and K.-L. Tsui, "Gini indices II and III: Two new sparsity measures and their applications to machine condition monitoring," *IEEE/ASME Trans. Mechatronics*, vol. 27, no. 3, pp. 1211–1222, Jun. 2022.
- [46] D. Wang, "Some further thoughts about spectral kurtosis, spectral L2/L1 norm, spectral smoothness index and spectral Gini index for characterizing repetitive transients," *Mech. Syst. Signal Process.*, vol. 108, pp. 360–368, Aug. 2018.
- [47] H. Huang, N. Baddour, and M. Liang, "Auto-OBSD: Automatic parameter selection for reliable oscillatory behavior-based signal decomposition with an application to bearing fault signature extraction," *Mech. Syst. Signal Process.*, vol. 86, pp. 237–259, Mar. 2017.
- [48] R. B. Randall, *Vibration-Based Condition Monitoring: Industrial, Automotive and Aerospace Applications*. Hoboken, NJ, USA: Wiley, 2021.
- [49] W. Chen, Z. Wang, H. Xie, and W. Yu, "Characterization of surface EMG signal based on fuzzy entropy," *IEEE Trans. Neural Syst. Rehabil. Eng.*, vol. 15, no. 2, pp. 266–272, Jun. 2007.
- [50] W. Chen, J. Zhuang, W. Yu, and Z. Wang, "Measuring complexity using FuzzyEn, ApEn, and SampEn," *Med. Eng. Phys.*, vol. 31, no. 1, pp. 61–68, Jan. 2009.
- [51] J. Lee, H. Qiu, G. Yu, and J. Lin, *Rexnord Technical Services (2007) IMS, University of Cincinnati. Bearing Data Set*. Moffett Field, CA, USA: NASA Ames Prognostics Data Repository, NASA Ames Research Center, 2007. [Online]. Available: <http://ti.arc.nasa.gov/project/prognostic-data-repository>
- [52] P. Castagliola and P. E. Maravelakis, "A CUSUM control chart for monitoring the variance when parameters are estimated," *J. Statist. Planning Inference*, vol. 141, no. 4, pp. 1463–1478, 2011.
- [53] H. Wang, Y. Chen, C. Chan, and J. Qin, "Application of residual-based cumulative sum control charts for detecting faults in autocorrelated processes," *J. Vibrot., Meas. Diagnosis*, vol. 32, no. 1, pp. 73–77, 2012.



Khandaker Noman received the B.Sc. degree from the Islamic University of Technology, Gazipur, Bangladesh, in 2014, the master's degree from Xi'an Jiaotong University, Xi'an, China, in 2017, and the Ph.D. degree from Shanghai Jiao Tong University, Shanghai, China, in 2021.

He is currently working as a Post-Doctoral Research Fellow with Northwestern Polytechnical University, Xi'an, China. His main research interests include signal processing, condition monitoring, fault diagnosis, and reliability analysis.



Yongbo Li (Member, IEEE) received the master's degree from Harbin Engineering University (HRBEU), Harbin, China, in 2012, and the Ph.D. degree in general mechanics from Harbin Institute of Technology (HIT), Harbin, in 2017.

He is currently an Associate Professor with the School of Aeronautics, Northwestern Polytechnical University, Xi'an, China. Prior to joining Northwestern Polytechnical University in 2017, he was a Visiting Student with the University of Alberta, Edmonton, AB, Canada. He currently holds five research grants from the National Natural Science Foundation of China, the Shaanxi Province Key Research Program, and the China Postdoctoral Science Foundation. His research interests include signal processing, fault feature extraction, and fault pattern identification.



Shun Wang received the B.Sc. degree in aircraft control and information engineering from Northwestern Polytechnical University, Xi'an, China, in 2020, where he is currently pursuing the M.S. degree in aerospace science and technology.

His research interests include entropy, signal processing, fault diagnosis, condition monitoring, and pattern identification.